Journal of Alloys and Compounds 509 (2011) 3889–3893

Contents lists available at ScienceDirect

Journal of Alloys and Compounds

journal homepage: www.elsevier.com/locate/jallcom

Self-assembled sandwich-like NiO film and its application for Li-ion batteries

J. Zhong, X.L. Wang*, X.H. Xia, C.D. Gu, J.Y. Xiang, J. Zhang, J.P. Tu*

State Key Laboratory of Silicon Materials and Department of Materials Science and Engineering, Zhejiang University, Hangzhou 310027, China

ARTICLE INFO

Article history:
Received 26 September 2010
Received in revised form
17 December 2010
Accepted 17 December 2010
Available online 28 December 2010

Keywords:
Nickel oxide
Self-assembled film
Anode
Li-ion battery

ABSTRACT

NiO film with sandwich-like morphology is fabricated on nickel foam by a simple ammonia-evaporation process. Ammonia plays a major role in controlling the final geometry during this template- and surfactant-free synthesis. The obtained NiO film is constructed by regular triangular prisms with side length of 500 nm. Each triangular prism is self-assembled by single crystalline platelets. As an anode for lithium ion battery, this NiO film electrode exhibits high discharge capacity and excellent cycling performance. The reversible capacity of the sandwich-like NiO film sustains 400 mAh g^{-1} even after 50 cycles at 2 C, much higher than that of the dense NiO film prepared by eletrodeposition (198 mAh g^{-1}). The high rate capability and reversibility of this NiO film can be attributed to its unique sandwich-like architecture.

1. Introduction

3d transition metal oxides (*M*-O, *M* is Fe, Co, Ni, and Cu) have been widely studied as anodes for lithium ion batteries due to their high theoretic capacity, excellent reversibility of electrode reaction and low cost [1–10]. Among these transition metal oxides, NiO has been paid much attention due to its attractive advantages such as high theoretic capacity (718 mAh g^{-1}), nontoxicity and low material cost.

In the past decades, many methods have been reported for the synthesis of NiO particles and films with various morphologies [11–37], which included nanoplates, nanorods, nanowires, nanotubes, 3D-rose like and hollow microsphere particles, and dense, porous, network structure films. Recently, self-assembled synthesis of hierarchical structured NiO particles have been developed [38–42]. For instance, concave polyhedron shaped NiO particles obtained by Zhou's group show potential application for batteries [43]. These particles look like regularly twisted triangular prisms and exhibit better reversibility than the nanoplates as electrode materials. However, in the case of powder materials for Li-ion batteries, the active materials should be mixed with ancillary materials such as carbon black and polymer binder. This process is tedious and may negate the benefits associated with the reduced particle size and introduce undesirable interfaces [44]. Therefore, the direct growth of hierarchical NiO films on current collector would be more promising for their applications in Li-ion batteries. To the best of our knowledge, there is little literature about NiO films with such structure.

In the present work, nickel foam-supported NiO film composed of sandwich-like regular triangular prisms was firstly synthesized by a facile ammonia-evaporation-induced method. The potential application of the as-prepared NiO film in Li-ion batteries was investigated and the effects of the sandwich-like regular triangular prism structure on the reversibility and rate capability of the electrode were also discussed.

2. Experimental

40 ml aqueous ammonia (25–28%) was added to 20 ml aqueous solution of $Ni(NO_3)_2{\cdot}H_2O$ (0.5 M) with vigorous stirring. The resulting homogeneous solution was transferred into a Petri dish. Nickel foam substrate pressed to thin plate was immersed in the above reaction solution. After heated at 90 °C for 3 h, the nickel foam substrate was covered with a green film. This green precursor film was washed with deionized water and ethanol for several times, and dried. Then the film was heated in a tube furnace at 350 °C for 2 h in flowing argon. The loading density of the film after heat treatment is 0.92 mg cm^{-2} calculated from the weight increment. A blank test was performed in a solution without nickel salt. After the reaction, the weight of the nickel foam did not change, indicating the nickel foam do not react with the solution. For comparison, a dense NiO film was also prepared on nickel foam substrate by an electrodeposition method reported by our group before [12].

The structure and morphology of the film were characterized by X-ray diffraction (XRD, RigakuD/max-3B), scanning electron microscopy (SEM, FEI Sirion-100) and transmission electron microscopy (TEM, JEOL JEM200CX). Electrochemical performances of the film were investigated with two-electrode coin-type cells (CR2025). The cells were assembled in an argon-filled glove box using the nickel foam-supported NiO films as working electrodes, Li foils as counter-electrodes, polypropylene films as separators, and an electrolyte of 1 M $LiPF_6$ in a 1:1 (w/w) mixture of ethylene carbonate and diethyl carbonate. The cells were galvanostatically discharged and charged at a rate of 2 C (1 C = 718 mA g^{-1}) in the voltage range

* Corresponding authors. Tel.: +86 571 87952856; fax: +86 571 87952573.
E-mail addresses: wangxl@zju.edu.cn (X.L. Wang), tujp@zjuem.zju.edu.cn, tujp@zju.edu.cn (J.P. Tu).

0925-8388/$ – see front matter © 2010 Elsevier B.V. All rights reserved.
doi:10.1016/j.jallcom.2010.12.151

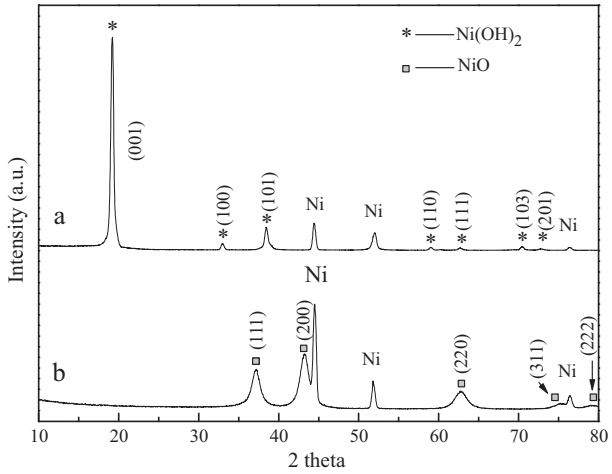

Fig. 1. XRD patterns of nickel foam-supported films (a) before and (b) after heat treatment.

of 0.01–3.0 V (*vs.* Li^+/Li) at 25 ± 1 °C. Cyclic voltammetry (CV) test was carried out using the CHI660C at a scanning rate of 0.5 mV s^{-1} between 0 and 3 V.

3. Results and discussion

Fig. 1 shows the XRD patterns of the as-prepared nickel foam-supporting films before and after heat treatment. For the sample before heat treatment, besides the peaks of the Ni substrate, all the diffraction peaks in the pattern (Fig. 1a) correspond to well-crystallized β-phase hexagonal nickel hydroxide (JCPDS Card No. 14-0117). The diffraction peak at 19.3°, which is indexed to (0 0 1) plane of β-$Ni(OH)_2$, is much stronger than the others. It implies the preferable growth of β-$Ni(OH)_2$ along ⟨0 0 1⟩ direction. In Fig. 1b, the diffraction peaks of the film after heat treatment can be well assigned to cubic NiO (JCPDS Card No. 47-1049). The reaction processes can be expressed below [40]. As is seen, the formation of NiO is resulted from the competition balance between reactions (1) and (2) [46]. The high concentration of dissolved ammonia in the initial solution brings excess NH_4^+ and NH_3, which react with Ni^{2+} to form $Ni(NH_3)_6^{2+}$. When heated at 90 °C, ammonia begins to evap-

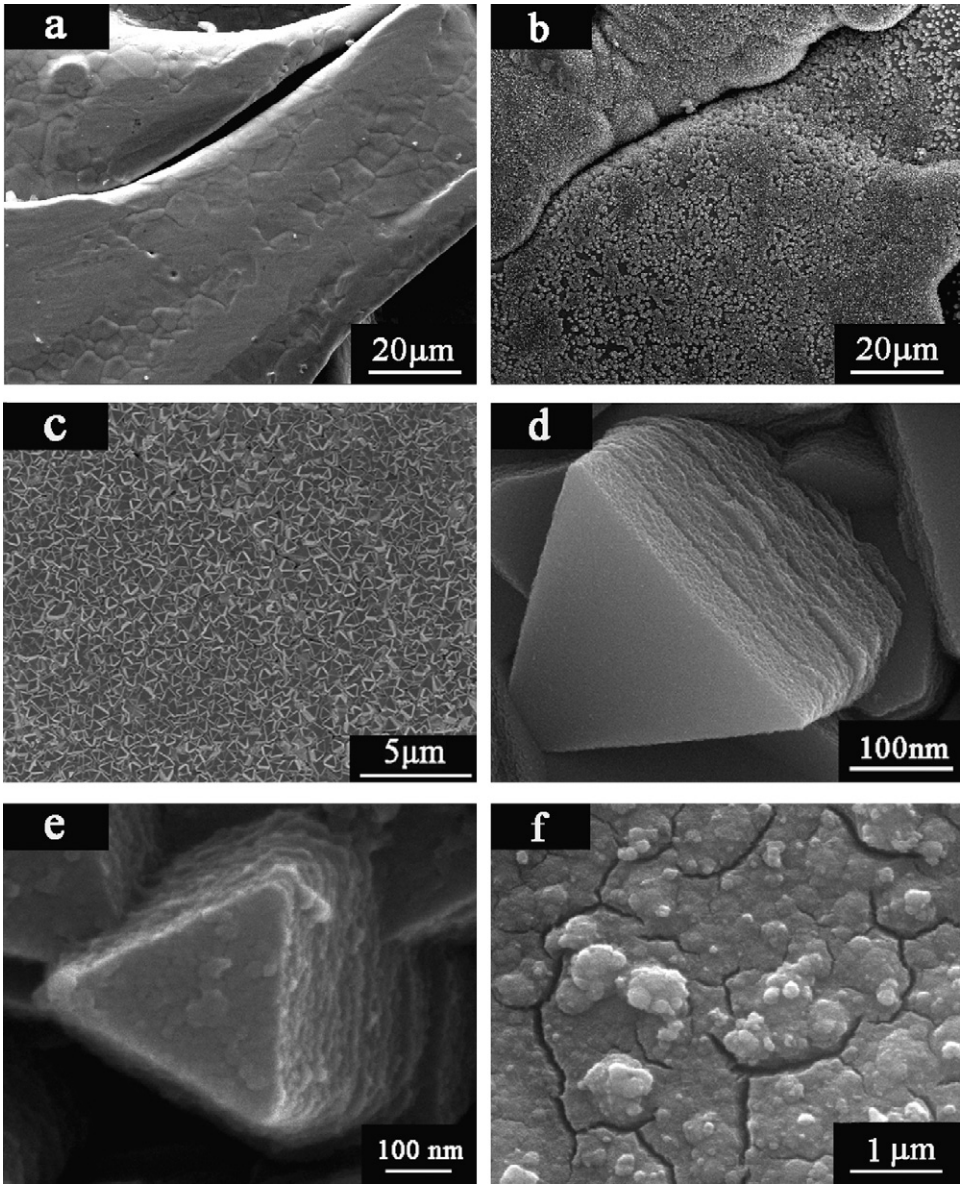

Fig. 2. SEM images of nickel foam-supported $Ni(OH)_2$ and NiO films: (a) bare nickel foam substrate, (b) overview of $Ni(OH)_2$ film, (c) top view of $Ni(OH)_2$ film, (d) a magnified image of a $Ni(OH)_2$ particle, (e) a magnified image of a NiO particle, and (f) the dense NiO film prepared by eletrodeposition.

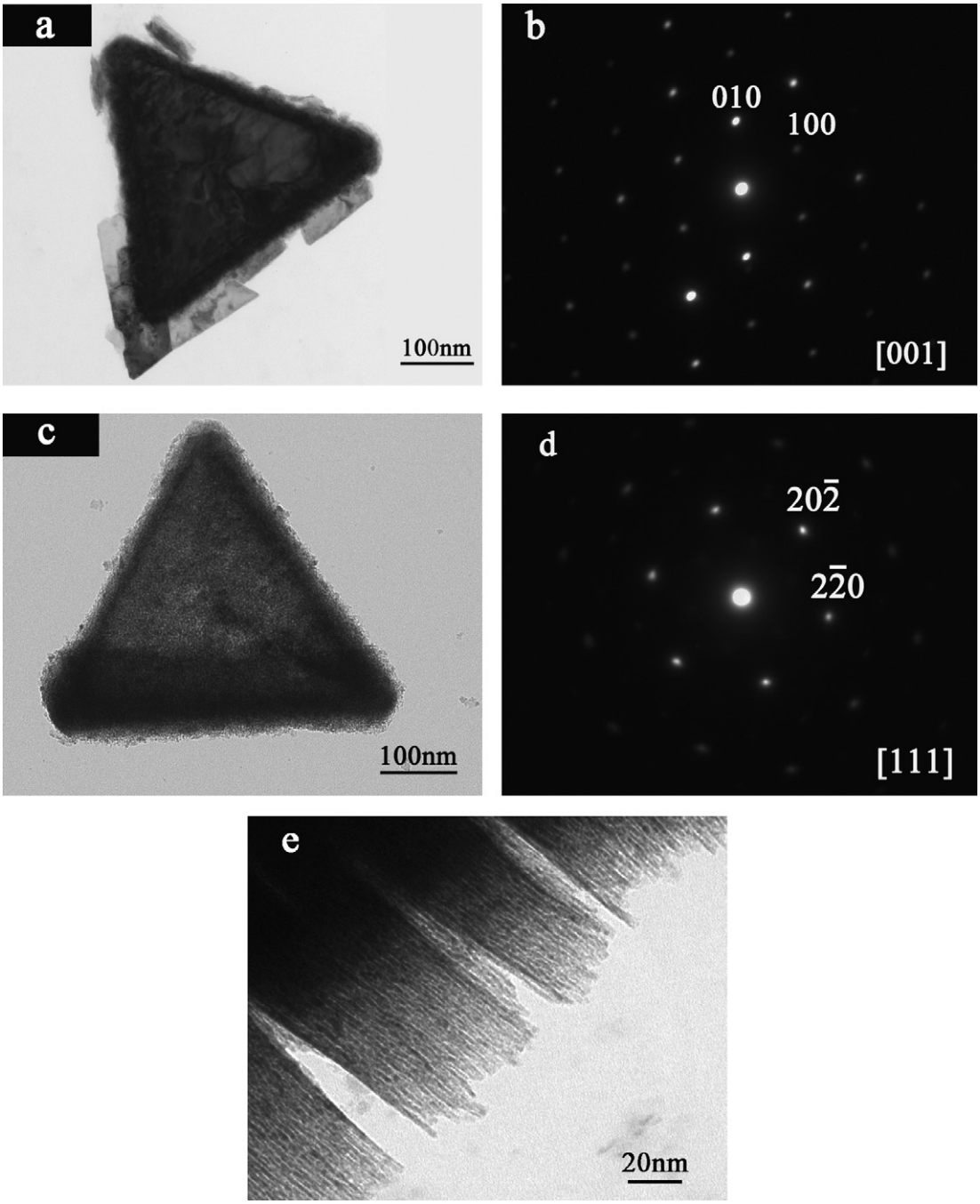

Fig. 3. TEM images and SAED patterns of (a) and (b) front view of the flakes of $Ni(OH)_2$, (c) and (d) NiO, and (e) side view of the flakes of NiO film.

orate and the hydrolysis of $Ni(NH_3)_6^{2+}$ occurs, forming $Ni(OH)_2$. At last, NiO is obtained by the thermal decomposition of $Ni(OH)_2$.

$$Ni^{2+} + 6NH_3 \rightarrow Ni(NH_3)_6^{2+} \quad (1)$$

$$Ni(NH_3)_6^{2+} + 2OH^- \xrightarrow{90\,^\circ C} Ni(OH)_2 \downarrow + 6NH_3 \quad (2)$$

$$Ni(OH)_2 \xrightarrow{350\,^\circ C} NiO + H_2O \quad (3)$$

Typical SEM images of the $Ni(OH)_2$ and NiO films are shown in Fig. 2. The nickel foam substrates are fully covered by plenty of homogeneous small particles (Fig. 2a and b). Fig. 2c is a top-view of the $Ni(OH)_2$ precursor film, revealing that this film is constructed by uniform and well-organized regular triangular prisms. The prisms are perpendicular to the surface of the substrate. The magnified image in Fig. 2d shows that each prism is composed from regular stacking of triangular platelets like a sandwich. The average side length of the triangular prism is about 500 nm. Fig. 2e shows the SEM image of NiO film. It can be seen that the morphology of NiO film is quite similar to that of the $Ni(OH)_2$ film, except for the rough surfaces and edges of the prisms.

TEM images of the flakes of the as-prepared films in Fig. 3a and b further confirm the triangular shape of $Ni(OH)_2$ and NiO. The corresponding SAED pattern of the $Ni(OH)_2$ displays a hexagonal symmetry, revealing that every $Ni(OH)_2$ triangular prism is a single crystal and the surface of the stacks is (0 0 1) plane of the hexagonal β-phase (Fig. 3b). It indicates that the $Ni(OH)_2$ nanoplates pile up together and grow along [0 0 1] direction, namely the *c*-axis of β-$Ni(OH)_2$. It is consistent with the (0 0 1) preferred orienta-

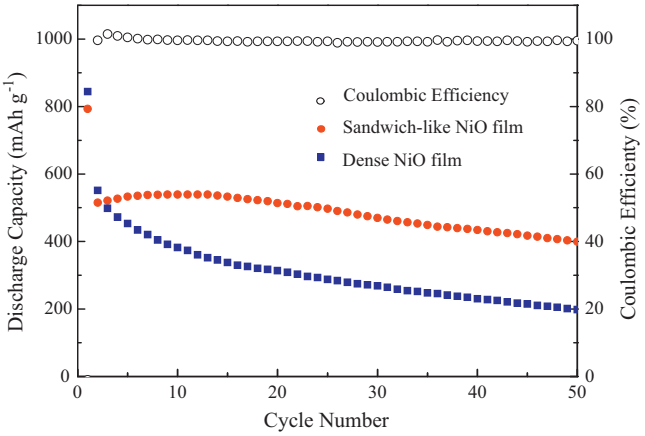

Fig. 4. Cycling performances of (a) the sandwich-like NiO film and (b) the dense NiO film; (c) coulombic efficiency of the sandwich-like NiO film during cycling.

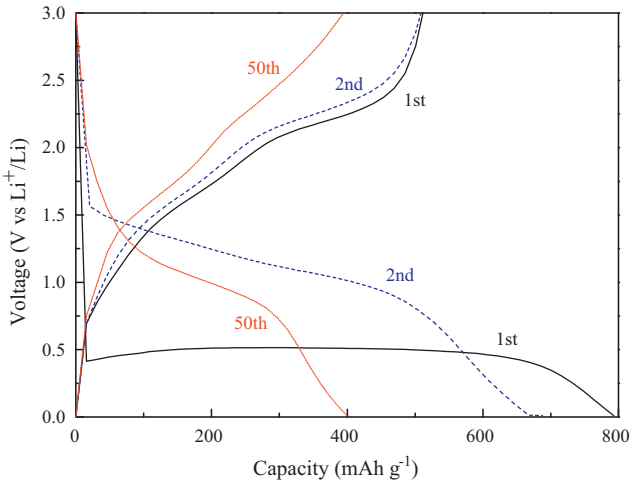

Fig. 5. Discharge/charge curves of the NiO film electrode at 1436 mA g^{-1} (2 C rate).

tion revealed by XRD. The SAED pattern of the NiO shows that each prism is constructed by single-crystalline NiO nanoplates with [1 1 1] axis perpendicular to the triangle face (Fig. 3d). The single-crystalline nature of the NiO nanoplates can be understood as a result of the conversion from $Ni(OH)_2$ to NiO with a relationship of $Ni(OH)_2$ [0 0 1] || NiO [1 1 1], since the symmetry of the lattice array in (1 1 1) plane of the fcc NiO is the same as that in (0 0 1) plane of the hexagonal β-$Ni(OH)_2$, and *d*-spacing of (2 0 0) plane (0.136 nm) in $Ni(OH)_2$ is close to that of (2 2 0) plane (0.147 nm) in NiO [47]. TEM image of the side view of the NiO flakes further verifies the lamellar feature (Fig. 3e). It is evident that each prism is resulted from the piling up of hundreds of thin plates. The thickness of a layer is less than 3 nm. These layers become not so uniform after the dehydration, explaining the rough and blurry edges of NiO.

It is considered that the formation of triangular prism is resulted from the self-assembled growth of $Ni(OH)_2$. In a typical $Ni(OH)_2$ molecule, the metal cations Ni^{2+} are located in the central spaces of oxygen octahedral from six hydroxyl groups. These octahedral then share their edges to form two dimensional (2D) sheets similar to the well-know mineral compound brucite $Mg(OH)_2$ [48]. In this experiment, ammonia controls the precipitation and the passivation of crystal surfaces. The nanostructures grow in a dynamic process with a gradual decreasing of pH value and ammonia concentration in the solution. And the final hierarchical nanostructure forms because of the different affinity that ammonia with different crystal plane [45].

As anode for lithium ion batteries, the electrochemical performances of the NiO film are evaluated by galvanostatically discharged–charged cycling and CV tests. Fig. 4 shows the capacity retention properties of the NiO film electrodes. The specific capacity for the sandwich-like NiO film electrode after 50 cycles is 400 mAh g^{-1} at a discharge current density of 1436 mA g^{-1} (2 C rate), which retains 78% of that in the 2nd cycle. Moreover, the coulombic efficiency of the electrode keeps over 98% after the 2nd cycle. But for the dense NiO film, the specific capacity after 50 cycles is only 198 mAh g^{-1}. By comparison, the sandwich-like NiO film exhibits much better capacity retention than the dense one.

Fig. 5 shows the discharge/charge curves of the NiO film electrode at 1436 mA g^{-1} (2 C rate). During the first discharge process, the voltage decreases steeply to 0.5 V where a plateau region sets in and continues until a discharge capacity of 630 mAh g^{-1} is reached. Another slope is observed at 0.4 V, with a total first discharge capacity of 793 mAh g^{-1}. The first charge capacity is 511 mAh g^{-1}, leading to the initial columbic efficiency of about 64.4%. Fig. 6 shows the second discharge/charge curves of the NiO film electrode at rates of 0.1 C, 1 C and 2 C. During this cycling at 2 C, the voltage plateaus appear at about 1.2 V and 2.2 V, respectively and the polarization occurs. Polarization also exists at rates of 0.1 C and 1 C. It can be seen that the difference of the polarization between 1 C and 2 C are not obvious. And the polarization in 0.1 C is smaller.

Cyclic voltammogram (CV) curves give complementary data to the galvanostatic cycling (Fig. 7). During the second cathodic/anodic scanning, the reduction peaks around 1.34 V and 1.0 V correspond to the formation of the SEI and the initial reduction of NiO to metallic Ni, respectively. The oxidation peak around 1.47 V and 2.28 V correspond to the partial decomposition of SEI and the decomposition of Li_2O, respectively. These voltage values are in agreement with NiO nanoparticle reported in precious literature [16]. Compared with the dense NiO film reported before [48], the separation between cathodic and anodic peaks of the sandwich-like NiO film in this work is smaller, indicating the weaker polarization and better reversibility.

The good electrochemical performances of sandwich-like NiO film can be attributed to the following reasons: first, the open space between the neighboring prisms and the layered structure can offer larger electrode/electrolyte contact area and shorter diffusion length of lithium ions. It can also accommodate the strain induced by the volume change during the charge and discharge process. Second, every prism contacts directly with the foam nickel substrate, which can enhance the conductivity of the electrode. Third, the stability of the large single-crystalline domains may enhance the

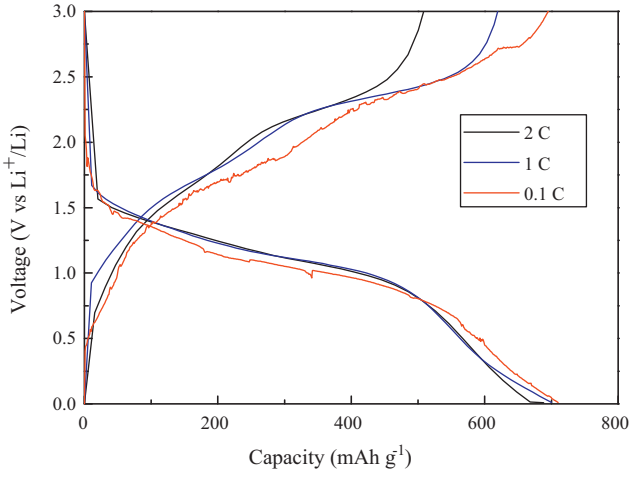

Fig. 6. The second discharge/charge curves of the NiO film electrode at rates of 0.1 C, 1 C and 2 C.

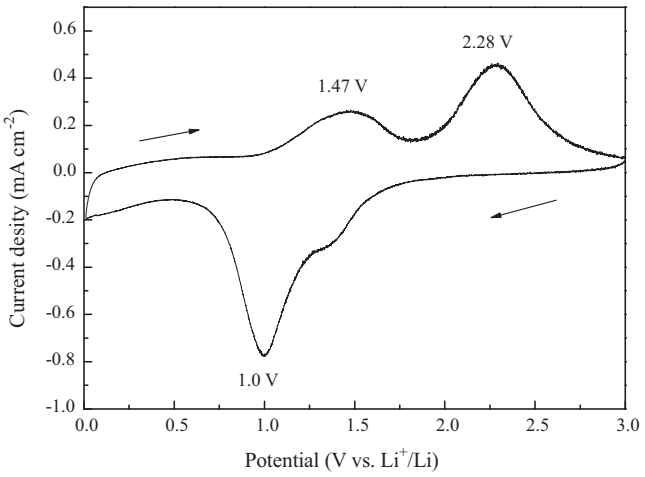

Fig. 7. Cyclic voltammograms of the NiO film electrodes at a scan rate of 0.5 mV s^{-1}

retention of the film [49]. What's more the nickel foam substrate leads to much more active material comparing with the metal-foil substrate [50]. As a result, this sandwich-like NiO film has potential application in the field of attractive power sources.

4. Conclusions

NiO film with regular triangular prisms was grown on the nickel foam substrate by a facile ammonia-evaporation method. The single-crystalline NiO nanoplates pile up together and form sandwich-like structures with the bottom sticking to the substrate. The ammonia plays the major role in controlling the sandwich-like structure during the self-assembly growth process. The resultant NiO film exhibits high rate capability and coulombic efficiency, as well as good cycling performance, indicating that this sandwich-like film would be a potential electrode for the next-generation lithium ion batteries. Moreover, the ammonia-evaporation fabrication of the $Ni(OH)_2$ and NiO films provide a promising approach to preparing 3d transition metal hydroxide/oxide thin-film electrodes.

References

[1] P. Piozit, S. Laruelle, S. Grugeon, L. Dupont, J.-M. Tarascon, Nature 407 (2000) 496.
[2] J.-M. Tarascon, M. Armand, Nature 414 (2001) 359.
[3] S. Grugeon, S. Laruelle, R. Herrera-Urbina, L. Dupont, P. Poizot, J.-M. Tarascon, J. Electrochem. Soc. 148 (2001) A285.
[4] D. Larcher, G. Sudant, J.-B. Leriche, Y. Chabre, J.-M. Tarascon, J. Electrochem. Soc. 149 (2002) A234.
[5] P. Poizot, S. Laruelle, S. Grugeon, J.-M. Tarascon, J. Electrochem. Soc. 149 (2002) A1212.
[6] C. Li, Z.S. Yu, S.M. Fang, H.X. Wang, Y.H. Gui, J.P. Xu, R.F. Chen, J. Alloys Compd. 475 (2009) 718.
[7] Q.T. Pan, K. Huang, S.B. Ni, F. Yang, S.M. Lin, D.Y. He, J. Alloys Compd. 484 (2009) 322.
[8] Y.J. Chen, M.C. Hsu, Y.C. Cai, J. Alloys Compd. 490 (2010) 493.
[9] K.F. Chen, Z. Lue, X.J. Chen, N. Ai, X.Q. Huang, B. Wei, J.Y. Hu, W.H. Su, J. Alloys Compd. 454 (2008) 447.
[10] H.B. Wang, Q.M. Pan, J.W. Zhao, W.T. Chen, J. Alloys Compd. 476 (2009) 408.
[11] E. Hosono, S. Fujihara, I. Honma, H.S. Zhou, Electrochem. Commun. 8 (2006) 284.
[12] X.H. Huang, J.P. Tu, X.H. Xia, X.L. Wang, J.Y. Xiang, L. Zhang, Y. Zhou, J. Power Sources 188 (2009) 588.
[13] X.H. Huang, J.P. Tu, X.H. Xia, X.L. Wang, J.Y. Xiang, Electrochem. Commun. 10 (2008) 1288.
[14] Y. Wang, Q.Z. Qin, J. Electrochem. Soc. 149 (2002) A873.
[15] Y. Wang, Y.F. Zhang, H.R. Liu, S.J. Yu, Q.Z. Qin, Electrochim. Acta 48 (2003) 4253.
[16] B. Varghese, M.V. Reddy, Y.W. Zhu, C.S. Lit, T.C. Hoong, G.V. Subba Rao, B.V.R. Chowdari, A.T.S. Wee, C.T. Lim, C.H. Sow, Chem. Mater. 20 (2008) 3360.
[17] Y.N. Nuli, S.L. Zhao, Q.Z. Qin, J. Power Sources 114 (2003) 113.
[18] K.F. Chiu, C.Y. Chang, C.M. Lin, J. Electrochem. Soc. 152 (2005) A1188.
[19] H.B. Wang, Q.M. Pan, X.P. Wang, G.P. Yin, J.W. Zhao, J. Appl. Electrochem. 39 (2009) 1597.
[20] Q.M. Pan, J. Liu, J. Solid State Electrochem. 13 (2009) 1591.
[21] A.A. Al-Ghamdi, W.E. Mahmoud, S.J. Yaghmour, F.M. Al-Marzouki, J. Alloys Compd. 486 (2009) 9.
[22] X.H. Huang, J.P. Tu, C.Q. Zhang, X.T. Chen, Y.F. Yuan, H.M. Wu, Electrochim. Acta 52 (2007) 4177.
[23] X.H. Huang, J.P. Tu, C.Q. Zhang, J.Y. Xiang, Electrochem. Commun. 9 (2007) 1180.
[24] F. Davar, Z. Fereshteh, M. Salavati-Niasari, J. Alloys Compd. 476 (2009) 797.
[25] M. Salavati-Niasari, F. Davar, Z. Fereshteh, J. Alloys Compd. 494 (2010) 410.
[26] A.C. Sonavane, A.I. Inamdar, P.S. Shinde, H.P. Deshmukh, R.S. Patil, P.S. Patil, J. Alloys Compd. 489 (2010) 667.
[27] X.H. Huang, J.P. Tu, Z.Y. Zeng, J.Y. Xiang, X.B. Zhao, J. Electrochem. Soc. 155 (2008) A438.
[28] X.H. Huang, J.P. Tu, X.H. Xia, X.L. Wang, J.Y. Xiang, L. Zhang, J. Power Sources 195 (2010) 1207.
[29] H.R. Liu, W.M. Zheng, X. Yan, B.X. Feng, J. Alloys Compd. 462 (2008) 356.
[30] T.-L. Lai, Y.-Y. Shu, G.-L. Huang, C.-C. Lee, C.-B. Wang, J. Alloys Compd. 450 (2008) 318.
[31] H.L. Wang, H.S. Casalongue, Y.Y. Liang, H.J. Dai, J. Am. Chem. Soc. 132 (2010) 7472.
[32] K. Matsui, T. Kyotani, Adv. Mater. 14 (2002) 1216.
[33] L.H. Zhuo, J.C. Ge, L.H. Cao, B. Tang, Cryst. Growth Des. 9 (2009) 1.
[34] D.N. Yang, R.M. Wang, J. Zhang, Z.F. Liu, J. Phys. Chem. B 108 (2004) 7531.
[35] P. Zhang, Z.P. Guo, S.G. Kang, Y.J. Choi, C.J. Kim, K.W. Kim, H.K. Liu, J. Power Sources 189 (2009) 566.
[36] X.H. Huang, J.P. Tu, C.Q. Zhang, F. Zhou, Electrochim. Acta 55 (2010) 8981.
[37] J.B. Sanjeev Das, Y.C. Seol, C.G. Kim, Park, J. Alloys Compd. 505 (2010) L19.
[38] L. Wang, Y. Zhao, Q.Y. Lai, Y.J. Hao, J. Alloys Compd. 495 (2010) 82.
[39] Q.L. Zhou, F. Gu, C.Z. Li, J. Alloys Compd. 474 (2009) 358.
[40] X. Ni, Y. Zhang, D. Tian, H. Zheng, X. Wang, J. Cryst. Growth 306 (2007) 418.
[41] C. Coudun, J.F. Hochepied, J. Phys. Chem. B 109 (2005) 6069.
[42] S.M. Zhang, H.C. Zeng, Chem. Mater. 21 (2009) 871.
[43] W. Zhou, M. Yao, L. Guo, Y.M. Li, J.H. Li, S.H. Yang, J. Am. Chem. Soc. 131 (2009) 2959.
[44] S.A. Needham, G.X. Wang, H.K. Liu, J. Power Sources 159 (2006) 254.
[45] Y.G. Li, B. Tan, Y.Y. Wu, Chem. Mater. 20 (2008) 567.
[46] X.Y. Deng, Z. Chen, Mater. Lett. 58 (2004) 276.
[47] D.B. Kuang, B.X. Lei, Y.P. Pan, X.Y. Yu, C.Y. Su, J. Phys. Chem. C 113 (2009) 5508.
[48] G.W. Brindley, S. Kikkawa, Am. Miner. 64 (1979) 836.
[49] J.C. Park, J. Kim, H. Kwon, H. Song, Adv. Mater. 21 (2009) 803.
[50] Y. Yu, C.H. Chen, J.L. Shui, S. Xie, Angew. Chem. Int. Ed. 44 (2005) 7085.